ELSEVIER

Polymer 43 (2002) 4403–4412

polymer

www.elsevier.com/locate/polymer

Structure and process relationship of electrospun bioabsorbable nanofiber membranes

Xinhua Zong[a], Kwangsok Kim[a], Dufei Fang[b], Shaofeng Ran[a], Benjamin S. Hsiao[a,*], Benjamin Chu[a,**]

[a]*Department of Chemistry, State University of New York at Stony Brook, Stony Brook, NY 11794-3400, USA*
[b]*Stonybrook Technology and Applied Research Inc., P.O. Box 1336, Stony Brook, NY 11790, USA*

Received 28 February 2002; received in revised form 5 April 2002; accepted 8 April 2002

Abstract

An electrospinning method was used to fabricate bioabsorbable amorphous poly(D,L-lactic acid) (PDLA) and semi-crystalline poly(L-lactic acid) (PLLA) nanofiber non-woven membranes for biomedical applications. The structure and morphology of electrospun membranes were investigated by scanning electron microscopy (SEM), differential scanning calorimetry (DSC), and synchrotron wide-angle X-ray diffraction/small angle X-ray scattering. SEM images showed that the fiber diameter and the nanostructured morphology depended on processing parameters such as solution viscosity (e.g. concentration and polymer molecular weight), applied electric field strength, solution feeding rate and ionic salt addition. The combination of different materials and processing parameters could be used to fabricate bead-free nanofiber non-woven membranes. Concentration and salt addition were found to have relatively larger effects on the fiber diameter than the other parameters. DSC and X-ray results indicated that the electrospun PLLA nanofibers were completely non-crystalline but had highly oriented chains and a lower glass transition temperature than the cast film.

Keywords: Electrospinning; Poly(lactic acid); Biodegradable nanofiber

1. Introduction

Linear aliphatic polyesters such as polyglycolide (PGA), polylactide (PLA) and their random copolymer poly(glycolide-*co*-lactide) (PGA-*co*-PLA), are often used as the base materials for implant devices, such as suture fibers and scaffolds for tissue engineering [1–3]. These materials meet several controlled release criteria, i.e. they are biocompatible and biodegradable, and they can provide high efficiency of drug loading. Many different techniques have been developed to produce nanostructured biodegradable articles such as microspheres, foams and films. It has been demonstrated that the molecular structure and morphology of PLA, PGA and their copolymers can play a major role in the degradation and mechanical properties of the final products [4,5]. The release profiles of entrapped drugs can be fine-tuned by controlling the degradation rate of the polymer matrix through molecular weight and molecular weight distribution, material composition, and porosity of the carriers [6,7].

Recently, the electrospinning method has attracted a great deal of attention to produce non-woven membranes of nanofibers. This process was first studied by Zeleny [8] in 1914 and patented by Formhals in 1934 [9]. In 1964, Taylor showed that at a critical voltage, the equilibrium shape of the suspended meniscus was a cone with a semi-vertical angle of 49.3° [10]. When the applied voltage exceeded this critical voltage, a stable jet of liquid could be ejected. The work of Taylor and others on electrically driven jets of the liquids inspired scientists to apply the same principle to polymeric systems [11–15]. Great efforts have been made to study the effects of processing parameters on the structure and morphology of electrospun fibers. For example, Doshi and Reneker correlated the electrospinning process and the physical properties of electrospun polymeric nanofibers [13]. They found that by reducing the surface tension, fibers could be produced without beads. A higher net charge density of the polymer solution could also yield thinner fibers with no beads. Studies were also made to investigate the formation mechanism of nanofibers during electrospinning. For example, Reneker et al. [14] characterized the

* Corresponding author. Tel.: +1-631-632-7793; fax: +1-631-632-6518.
** Corresponding author. Tel.: +1-631-632-7928; fax: +1-631-632-6518.
E-mail addresses: bhsiao@notes.cc.sunysb.edu (B.S. Hsiao); bchu@notes.cc.sunysb.edu (B. Chu).

0032-3861/02/$ - see front matter
PII: S0032-3861(02)00275-6

bending instability in the charged liquid jet during electrospinning. Shin et al. [15] studied the instability of the electrically forced fluid jet and argued that the essential mechanism of electrospinning was a rapidly whipping fluid jet.

The most studied polymer system by electrospinning is perhaps polyethylene oxide (PEO). However, the relationships between processing parameters and microstructures in the electrospun PEO membrane are still not well understood. Recently, Deitzel et al. [16] pointed out that the crystalline structure of the electrospun PEO fibers was not well developed in spite of the good crystallization ability of pure PEO, especially when under elongational flow. Some unique microstructures have been observed in other types of polymers by electrospinning. For example, Buchko et al. [17] electrospun a silk-like polymer with fibronectin functionality (SLPF) and reported a shish–kebab structure in the filament morphology.

The electrospinning technology is well suited to process natural biomaterials and synthetic biocompatible or bioabsorbable polymers for biomedical applications. Potential applications of these non-woven nanostructured membranes include filtration, anti-adhesion membranes, wound dressing scaffolds, and artificial blood vessels. In the present study, we have investigated the effects of varying the processing parameters in electrospinning on the microstructure of biodegradable amorphous poly(D,L-lactide) (PDLA) and semi-crystalline poly(L-lactide) (PLLA) membranes. These two samples were chosen because the degree of crystallinity in the sample can significantly hinder the degradation rate, which is the subject of our research interest. The target application of these membranes is for the prevention of surgery induced-adhesions. Scanning electron microscopy (SEM), differential scanning calorimetry (DSC), wide-angle X-ray diffraction (WAXD) and small angle X-ray scattering (SAXS) techniques were used to investigate the structure and morphology of the electrospun PDLA and PLLA nanofibers. We have also demonstrated that the electrospinning technique could be used to load medicines, such as antibiotics, into the membranes.

2. Experimental

The amorphous poly(D,L-lactic acid) (PDLA) sample with an inherent viscosity of 0.55–0.75 dl/g was purchased from Birmingham Polymers, Inc. (Birmingham, AL). This polymer contained a weight average molecular weight (M_w) of 1.09×10^5 g/mol and a polydispersity index (M_w/M_n) of 1.42. The semi-crystalline poly(L-lactic acid) (PLLA) sample was an experimental material produced from DuPont, having a weight average molecular weight (M_w) of 1.0×10^5 g/mol, a polydispersity index (M_w/M_n) of 2.0 and $\%R \sim 5$. For PDLA, dimethyl formamide (DMF) was typically used as the solvent to prepare the polymer solutions at different concentrations for electrospinning.

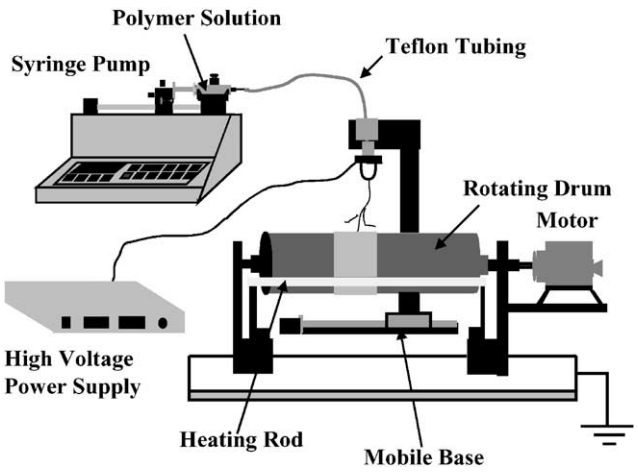

Fig. 1. Schematic diagram of the electrospinning apparatus for manufacturing nanofiber-structured membranes.

For semi-crystalline PLLA, a mixed solvent of methlyene chloride and dimethyl formamide with a typical weight ratio of 1.5 (methylene chloride: dimethyl formamide) was used to dissolve the polymer. Three kinds of salts were used to change the charge density of the solutions during electrospinning: sodium chloride, sodium phosphate and potassium phosphate. An antibiotic drug Mefoxin ((6*R-cis*)-3-[[aminocarbonyl)oxy]-methyl]-7-methoxy-8-oxo-7-[(2-thienylacetyl)amino]-5-thia-1-azabicyclo[4.2.0]oct-2-ene-2-carboxylic acid, Merck Inc.), a weak ionic compound, was also added to the solution for electrospinning.

A schematic diagram of the electrospinning device for manufacturing fibers of small diameters is shown in Fig. 1. The polymer solution was delivered by a programmable pump (Harvard Apparatus, MA) to the exit hole of the electrode (spinneret with a hole diameter of 0.7 mm). The achievable flow rate range was 5–100 μl/min. A positive high-voltage supply (Glassman High Voltage Inc.) was used to supply the voltage in a range of 0–30 kV. The collecting plate was on a rotating drum, which was grounded and controlled by a stepping motor. The distance of electric field was fixed at 150 mm. A heating rod was used to accelerate solvent evaporation. The recovered samples were placed in a vacuum oven at room temperature to fully eliminate the solvent.

The viscosity of polymer solution was determined by using a Brookfield digital viscometer (model LVTDCP) at 25.0 °C. The morphology of the resulting nanofiber membranes was examined with SEM (JEOL JSM5300) after gold coating. The average diameter and the diameter distribution were obtained by using a custom code image analysis program to analyze the SEM images. DSC measurements were carried out with a Perkin Elmer DSC7 instrument. About 5 mg of samples were hermetically sealed in an aluminum pan for these measurements. Typical temperature profiles for the DSC study were as follows. The samples were heated from 0 to 200 °C at a rate of 20 °C/min

and held for 3 min at 200 °C; the samples were then cooled down to 0 °C at the same rate. Synchrotron WAXD/SAXS measurements were carried out at the X3A2 SUNY beamline, National Synchrotron Light Source (NSLS) at Brookhaven National Laboratory (BNL). The wavelength used was 1.544 Å. Two Fuji HR-V imaging plates ($200 \times 250\ mm^2$) were used to collect the SAXS/WAXD data simultaneously. The SAXS angle was calibrated by a silver behnate standard, and the WAXD angle was calibrated by using a silicon standard.

The drug release rate from the membrane containing Mefoxin was studied by a UV–visible spectrophotometer (Perkin–Elmer Lambda 12 spectrophotometer) at the wavelength of 234 nm. The membrane sample was incubated in 20 ml (pH 7.4) phosphate buffer at room temperature.

3. Results and discussion

3.1. Electrospinning processing parameters

The following variables including solution properties (concentration and ionic salt addition) and processing parameters (applied electric field and solution flow feeding rate) have been examined. Their relationships with the membrane microstructure are summarized below.

3.1.1. Electric field effect

It has been observed that the shape of the initiating droplet on the exit hole of the electrode can be changed by several electrospinning variables such as applied voltage, viscosity and feeding rate of the polymer solution. We confirm that an increase in the electrospinning voltage can alter the shape of the initial droplet. Consequently, the resulting fiber morphology can be changed from a typical cylindrical shape to a beaded or string-of-pearls structure. The electric field effect can be understood by the following argument. The jet initiation is a self-accelerating process. Once an electric field is applied on the droplet of the polymer solution at the tip of the spinneret, the surface of the liquid becomes charged via the motion of ions through the liquid. When the electric field is high enough such that the electric force overcomes the forces associated with the surface tension, a quasi-stable, straight and electrically charged jet is ejected. The balance between the surface tension and the electric force is critical to determine the initial cone shape of the polymer solution at the tip of the spinneret. For example, for a PDLA solution of 30 wt% at a feeding rate of 20 μl/min, the morphologies in the membranes obtained under different accelerating voltages (20, 25, and 30 kV) are shown in Fig. 2. The initiating jet was formed when the voltage exceeded 16 kV, but the jet was not stable at voltages below 20 kV. At 20 kV, the diameter of the droplet was found to be larger than the hole diameter of the spinneret. The jet was initiated from the

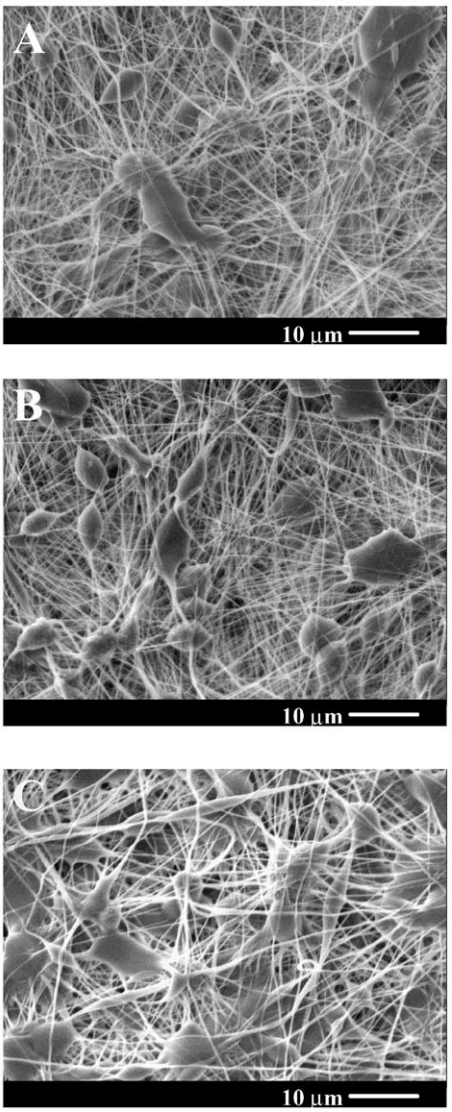

Fig. 2. Electric field effect on microstructures of the electrospun PDLA membranes at (A) 20 kV; (B) 25 kV and (C) 30 kV (concentration at 30 wt% PLA/DMF and feeding rate at 20 μl/min).

droplet suspended at the end of the spinneret. The hemispherical surface of the solution was elongated to form a conical shape (Taylor Cone). The Taylor cone was maintained at the bottom of the droplet even when the feed of the PDLA solution to the tip of the spinneret was faster than the jet could carry the fluid away. The resulting fibers are shown in Fig. 2A, which show a structure with only few beads on the fibers. When the applied voltage was increased, the jet velocity was increased and the solution was removed from the tip more quickly. As the volume of the droplet on the spinneret became smaller, the Taylor cone shape oscillated and became asymmetrical at 25 kV. Under this condition, beaded fibers were prone to form (Fig. 2B). The diameters of the beads were found to be smaller and the average distance between the beads on the fibers became shorter at 25 kV. With a further increase in voltage, the droplet at the tip of the spinneret disappeared almost

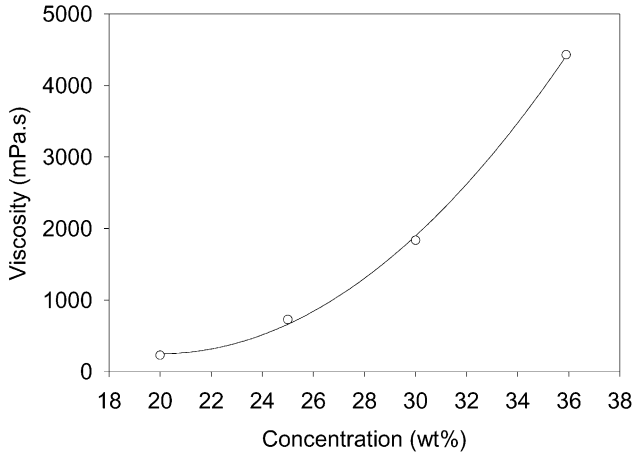

Fig. 3. Relationship between concentration and corresponding viscosity in PDLA/DMF solution.

completely and the jet was initiated directly from the tip. It appeared that the actual jet initiation occurred at some point inside the spinneret at an applied voltage of 30 kV. The corresponding fiber morphology is shown in Fig. 2C, which exhibits a larger average diameter at higher voltage. The shape of the beads was also seen to gradually change from spindle-like to spherical-like.

3.1.2. Concentration effect

Drastic morphological changes were found when the concentration of the polymer solution was changed. In other words, the concentration or the corresponding viscosity was one of the most effective variables to control the fiber morphology. Fig. 3 shows the range of concentrations used in this study for PDLA in dimethyl formamide and the corresponding viscosities. It is interesting to note that over a decade in viscosity can be obtained by varying the polymer concentration from 20 to 40 wt%. The SEM images of the membranes spun from the PDLA solutions of different viscosities are shown in Fig. 4 (under a voltage of 20 kV). We found that it was impossible to collect a continuous fiber at a concentration below 20 wt%. A mixture of large beads (drops) and fibers was generated by electrospinning the PDLA solution at concentrations below 20 wt%. In contrast, at concentrations higher than 40 wt%, the electrospinning process was hard to maintain due to the high viscosity of the solution, i.e. the droplet was dried out before the constant jet could be formed. In Fig. 4, the SEM images demonstrate the two extreme cases in the membrane morphology as a function of solution concentration. The membrane morphology is seen to change gradually from the full beads structure (Fig. 4A electrospun at the lowest solution viscosity) to the uniform fiber-structure (Fig. 4D, at the highest solution viscosity). We found that the more viscous the solution became (lower than the process limiting concentration), the more uniform the fibers were formed. In addition, the diameters of the beads became bigger and the average distance between the beads increased as the

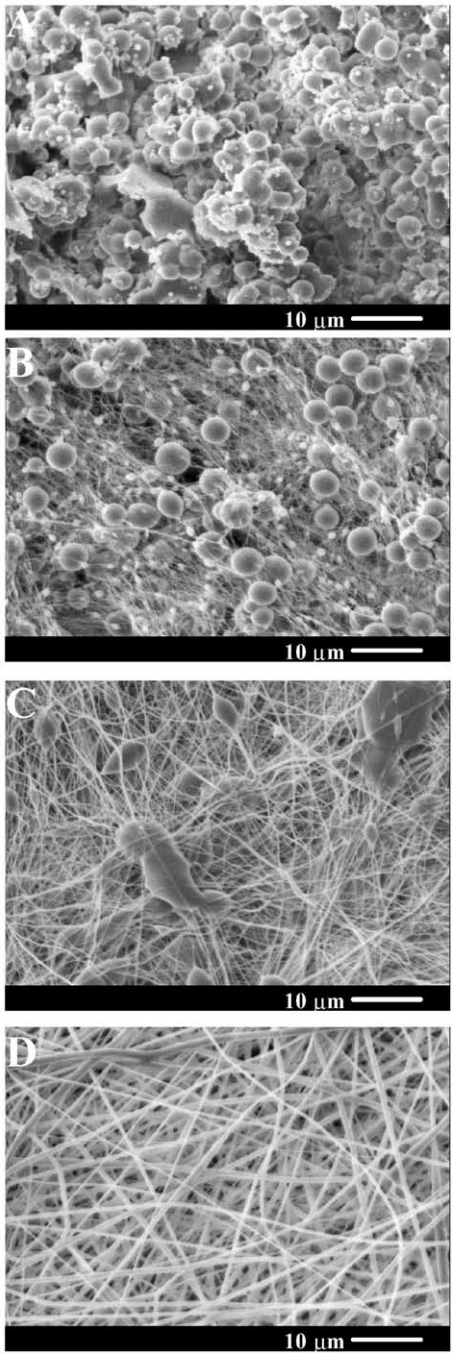

Fig. 4. Concentration effect on microstructures of electrospun PDLA nanofibers at voltage of 20 kV, feeding rate of 20 μl/min, and concentration of (A) 20 wt%; (B) 25 wt%; (C) 30 wt% and (D) 35 wt%.

viscosity of the PDLA solution increased. Meanwhile, the shape of the beads also changed from spherical to spindle-like. We offer the following reason to explain the concentration effect on the membrane morphology during electrospinning. We argue that, at lower concentrations, electrospun fibers are harder to dry before they reach the collection drum. The presence of junctions and bundles in the fibers electrospun from 20 to 30 wt% of PDLA solutions by SEM provides the evidence that the polymer fibers are

still wet at the time that they reach the collection drum. As the wet fibers are no longer strained by the electric field when they are laid on the ground, they can undergo a solidification process as a result of the surface tension and the relaxation process controlled by the viscoelastic property of the wet fibers. This process would result in the undulating morphology as seen in Fig. 4(A)–(C). In contrast, at higher concentrations, the electrospun fibers are mostly dried by the time they are collected. In general, we find that the effect of the electric field is opposite to the effect of viscosity in controlling the morphology of the electrospun membranes. To obtain a uniform fiber-structure, higher polymer concentration and lower electrical field strength are preferred.

3.1.3. Effects of ionic salt addition

Most drugs and proteins are soluble in water and form charged ions. As we intend to use the electrospun biodegradable membranes for medical applications, such as anti-adhesion barriers and drug release devices, it is important to investigate the effects of salt addition on the resulting morphologies of electrospun fibers. In this section, we demonstrate that very different morphologies of the electrospun fibers could be obtained when different salts were added into PDLA polymer solutions for electrospinning.

Fig. 5 shows the effects of three kinds of salts on the morphology of electrospun membranes. All results were obtained by electrospinning of PDLA/solvent/salt solutions at a voltage of 20 kV. If we compare Fig. 4C (30 wt% PDLA without salt at 20 kV) with Fig. 5, we find that no beads-on-string structure is formed for the solution with the addition of 1 wt% salts. All the resulting fibers exhibit a uniform diameter ranging from 200 to 1000 nm. This behavior can be explained as follows. The addition of salts results in a higher charge density on the surface of ejected jet during spinning, thus more electric charges are carried by the electrospinning jet. As the charges carried by the jet increase, higher elongation forces are imposed to the jet under the electrical field. It is known that the overall tension in the fibers depends on the self-repulsion of the excess charges on the jet. Thus, as the charge density increases, the beads become smaller and more spindle-like. The diameter of the final fibers also becomes substantially smaller.

In Fig. 5, we observe that different salts have different effects on the final fiber diameter. The fibers electrospun from the 30 wt% PDLA solution with 1 wt% NaCl exhibited the smallest average diameter of around 210 nm, while the fibers electrospun from the solution with 1 wt% KH_2PO_4 had the largest average diameter of around 1000 nm. The fibers spun from the solution with 1 wt% NaH_2PO_4 exhibited an average diameter of around 330 nm. Further image analysis revealed that a unimodal distribution of fiber diameters was obtained from membranes spun from the PDLA solutions with 1 wt% NaH_2PO_4 and NaCl (Fig. 6).

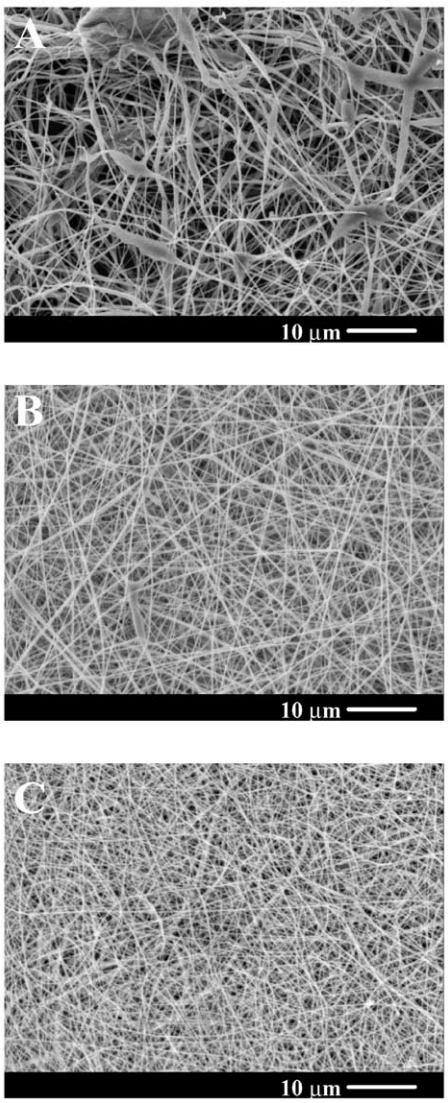

Fig. 5. SEM images of PDLA membranes fabricated by electrospinning of a 30 wt% solution at voltage of 20 kV, feeding rate of 20 μl/min and with 1 wt% of (A) KH_2PO_4; (B) NaH_2PO_4 and (C) NaCl.

This effect can be understood as follows. Besides the density of the charges carried by the jet, the size of the ions has an important impact on the resulting fiber diameter. Ions with smaller atomic radius have a higher charge density and thus a higher mobility under an external electric field. In this study, sodium and chloride ions have smaller radius than potassium and phosphate ions. Thus the elongational forces imposed on the jet with sodium chloride should be higher than that with potassium phosphate. Therefore, the electrospun fibers from the PDLA solution with 1 wt% NaCl possessed the smallest average fiber diameter, while the fibers spun from the solution with 1 wt% KH_2PO_4 had the largest fiber diameter.

3.1.4. Feeding rate effect

As we mentioned earlier, a certain minimum value of the solution volume suspended at the end of the spinneret

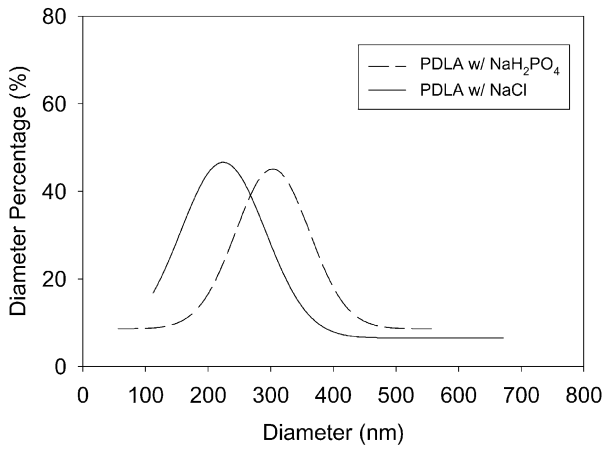

Fig. 6. Fiber diameter distributions of PDLA membranes electrospun at voltage of 20 kV, feeding rate of 20 μl/min and with 1 wt% of (- - -) NaH_2PO_4, (—) NaCl.

should be maintained in order to form an equilibrium Taylor cone. Therefore, different morphology can be obtained with the change in feeding rate at a given electric field. Fig. 7 shows the effect of the feeding rate on the morphology of the electrospun fibers from a 25 wt% PDLA solution with 1 wt% KH_2PO_4 at 20 kV. It was found that the lower the solution feeding rate was, the smaller the fibers with spindle-like beads were formed (Fig. 7A). Relatively large fiber diameters and beads were seen in fibers spun from a higher solution feeding rate (75 μl/min), as shown in Fig. 7B. This behavior can be explained as follows. Since the droplet suspended at the end of the spinneret is larger with a higher feeding rate, the jet of the solution can carry the fluid away with a faster velocity. As a result, the electrospun fibers are harder to dry before they reached the collection drum. This can result in large beads and junctions in the final membrane morphology (Fig. 7B).

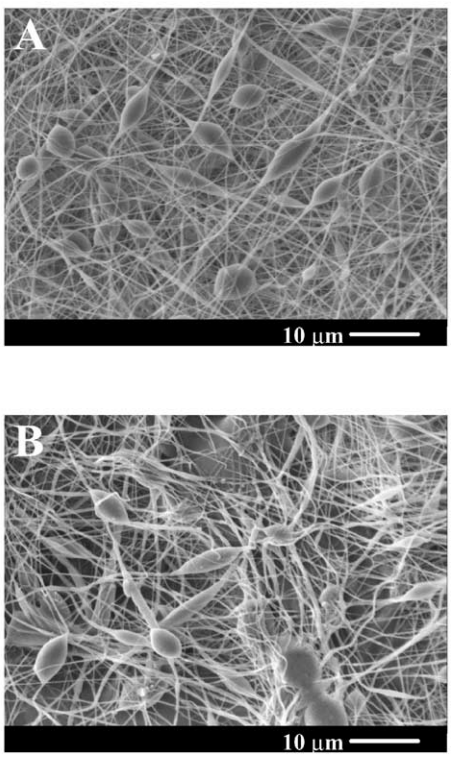

Fig. 7. SEM images showing the variation of beaded fibers at different feeding rates: (A) 20 μl/min; (B) 75 μl/min. The applied voltage was 20 kV and concentration was 25 wt% with 1 wt% KH_2PO_4.

3.2. Structure and property characterizations of electrospun membranes

3.2.1. Thermal properties

Fig. 8 shows the DSC thermograms of the as-received semi-crystalline PLLA resin and the electrospun PLLA membranes dried under vacuum at room temperature. For comparison, the thermogram of a quenched sample, which was prepared by first melting PLLA at 220 °C and then rapidly quenching with ice water, is also shown in Fig. 8. It is interesting to note that the as-received PLLA exhibits a crystallinity of 35.5%, whereas the electrospun PLLA membrane exhibits significantly lower values of crystallinity (if any), the glass transition temperature and the melting temperature. (Although not shown here, we found that the glass transition temperature of the electrospun non-crystallizable PDLA membrane was also reduced.) In addition, the electrospun membrane shows a large crystallization peak at 103 °C, but the quenched samples does not show any apparent crystallization peak under the temperature scan with the same heating rate (20 °C/min). This suggests that cold crystallization of the electrospun membranes during heating is enhanced probably due to the chain orientation. The decrease in glass transition temperature can be attributed to the very large surface to volume ratio of the electrospun membranes having air as the plasticizer. The extent of crystallinity in electrospun PLLA membrane is very low indicating that the majority of the chains are in the non-crystalline state. This can be understood as the rapid solidification process of stretched chains

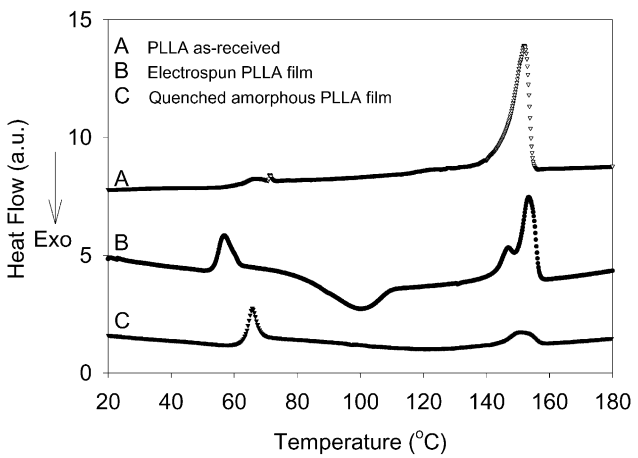

Fig. 8. DSC thermograms of (A) as-received PLLA; (B) electrospun PLLA dried at room temperature and (C) quenched PLLA in ice water.

under high elongational rate during the later stages of electrospinning may hinder the development of crystallinity as the chains do not have time to form crystalline registration. The decrease in crystallinity and the state of the oriented amorphous chains in the electrospun PLLA membranes will further be confirmed by X-ray examination.

3.2.2. Simultaneous WAXD and SAXS study

Fig. 9A shows the 2D WAXD pattern of an electrospun non-woven PLLA membrane. No crystalline peak is seen, which confirms that electrospinning almost completely retards the crystallization process of PLLA (the fully crystallized PLLA usually exhibits about 30% crystallinity with distinct crystalline reflections in WAXD). Although no orientation is seen from the non-woven membrane, strong scattering anisotropy in WAXD can be found in the aligned bundle samples (not shown here). This suggests that although the polymer chains are non-crystalline in the nanofibers they are highly oriented. The retardation of crystallization due to electrospinning has been first noted by Liu et al. [18] in the electrospun poly(*meta*-phenylene isophthalamide) nanofibers and was also reported by Deitzel et al. [16] in the study of crystallizable PEO nanofibers. It

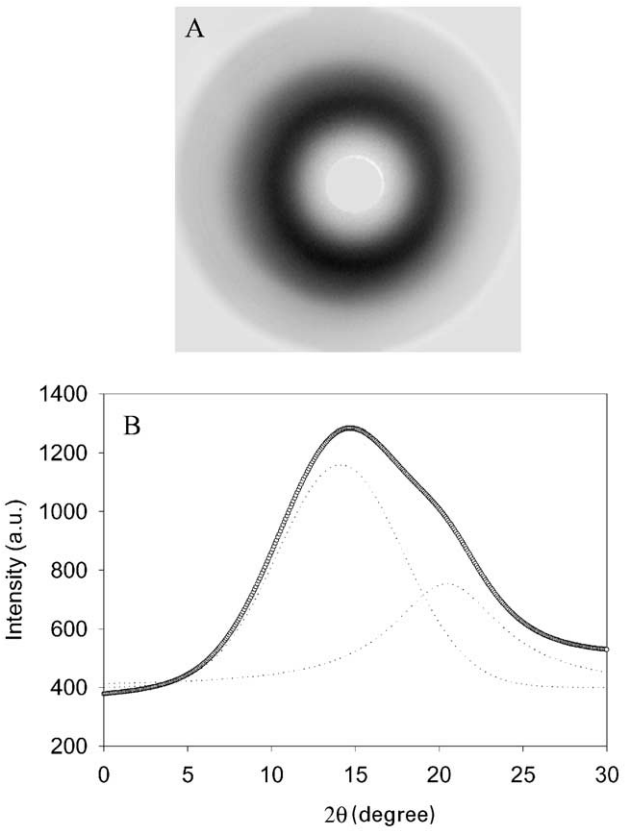

Fig. 9. (A) WAXD pattern of electrospun PLLA membranes dried at room temperature; (B) the integrated intensity profile from the WAXD pattern (the two dotted-line peaks represent the Gaussian fits for the amorphous background using the program Grams/32 Spectral Notebase™).

appears that this retardation of crystallization during electrospinning is universal, as we have observed similar behavior in several other semi-crystalline polymer solutions including pure poly(glycolide) and polyacrylonitrile. We attribute the retardation process to rapid solidification of stretched chains at high elongational rates during the later stages of electrospinning, which significantly hinders the formation of crystals. In other words, the stretched chains do not have enough time to organize into suitable crystal registration before they are solidified.

Fig. 9B represents the integrated intensity profile of the 2D WAXD pattern in Fig. 9A. The two dotted-line peaks represent the Gaussian fits of the amorphous background using the program Grams/32 Spectral Notebase™ (noted that a single Gaussian or Lorentzian peak cannot fit the amorphous profile). We note that the observed amorphous scattering profile from the electrospun PLLA membrane is not the same as that from the quenched amorphous PLLA film. In the electrospun fiber, the chains are highly oriented, but in the quenched amorphous film, the chains are in the random-coil state. The high degrees of molecular orientation in electrospun PEO fibers were also observed by Deitzel et al. and Larrondo et al. [16,19]. It is clear that the oriented PLLA chains in the nanofibers do not have any helical conformation, which is typically observed in the varying crystal forms [20]. Similar metastable states of highly oriented but non-crystalline chains between the amorphous and crystalline states have also been observed in other polymer fibers such as iPP and Kevlar [21,22].

After annealing at 55 °C for 24 h, the electrospun PLLA membrane exhibits two strong crystalline reflection peaks (Fig. 10). The integrated intensity profile of the 2D WAXD pattern is also shown in Fig. 10. The two peaks at 2θ values of 16.4 and 18.7°, which can be indexed as 110 and 131 reflections, agree very well with the values reported by Ikada et al. for the α form of the PLLA crystal having a pseudo-orthorhombic unit cell with dimensions ($a = 1.07$ nm, $b = 0.595$ nm, and $c = 2.78$ nm). This unit cell structure consists of two 10_3 helices [19]. The diffraction peaks appeared after annealing further confirmed that the electrospun PLLA fibers were in a metastable state. Thermal annealing improves the crystallographic packing of the PLLA chains.

Fig. 11A is the SAXS pattern of the as-spun PLLA membrane. The SAXS pattern of the annealed sample at 55 °C for 24 h is shown in Fig. 11B. Both patterns show strong diffuse scattering near the beam stop. Since the electrospun fibers are randomly oriented in the membrane, it is easy to understand that the pattern represent scattering from fibers of all directions. The interpretation of the scattering in SAXS is somewhat complicated since it may contain several contributions including the microfibrillar structure, surface reflection/scattering of the nanofibers and void morphology. Since no trace of discrete scattering (that would indicate the lamellar morphology) even for

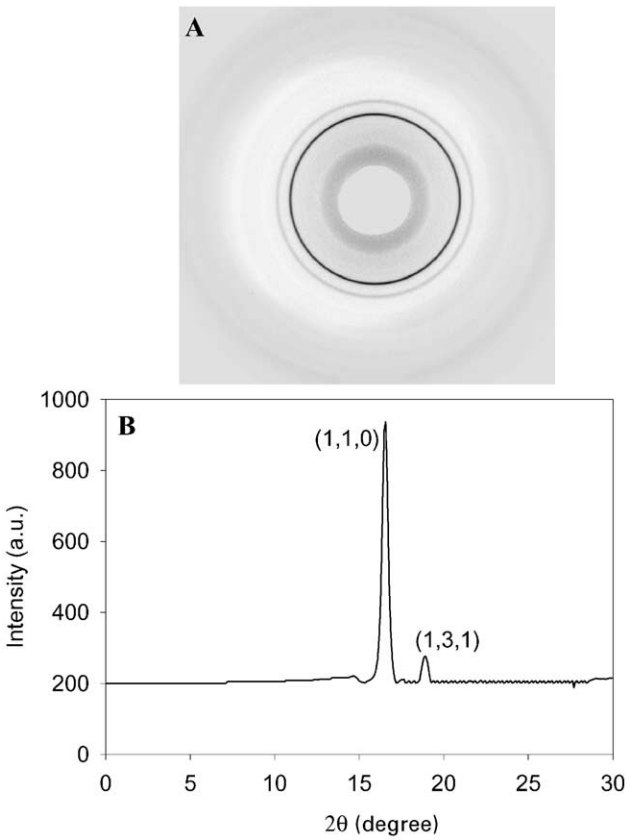

Fig. 10. (A) WAXD pattern of electrospun PLLA membranes annealed at 55 °C for 24 h; (B) the integrated intensity profile from the WAXD pattern.

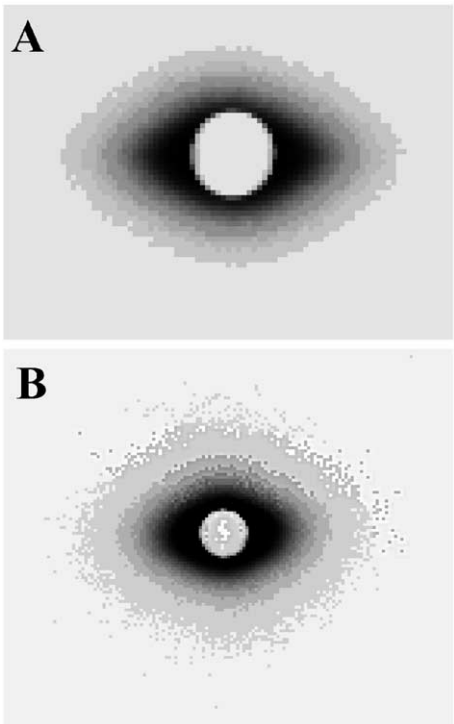

Fig. 11. SAXS patterns of (A) electrospun PLLA membranes dried at room temperature; (B) membrane annealed at 55 °C for 24 h.

the annealed sample was observed, we conclude that the scatterers in the electrospun PLLA fibers have a microfibrillar structure. In other words, we see no evidence of shish–kebab microstructure present in the electrospun PLLA fibers, which has been seen by Buchko et al. [17] for the sample of SLPF. Transmission electron microscopy (TEM) image was also taken for the annealed electrospun PLLA sample and confirmed that no shish–kebab structure are present in the PLLA nanofibers (data not shown).

3.2.3. Drug loading and release

As we mentioned earlier that most drugs and proteins are charged, it is very important to investigate the charge effect due to drug on the structure and morphology of electrospun membranes and the corresponding release profile. Fig. 12A shows the SEM image of electrospun PDLA membrane containing Mefoxin, one of the most popular antibiotics. The resulting membrane exhibits very uniform nanofiber-structures with an average diameter of 160 nm. The membrane also contains a comfortable texture for handling ability.

Since the nanofibers contain a very large surface to volume ratio and a short diffusion passage length, the degradation properties (in water) and drug release profiles of the electrospun membranes are very different from those of the bulk films with the same sample thickness. The unique nanostructured morphology of the membranes could provide several advantages for controlled delivery of drugs, proteins or even cells over the bulk films. In vitro drug release profile (Mefoxin) of the PDLA membranes in a 20 ml buffer solution is shown in Fig. 12B. This profile was determined with the UV spectroscopic technique by measuring the absorbance at 234 nm as a function of time. Fig. 12B shows that for the first 48 h, the entrapped drug was completely released from the membrane. The drug was released due to the concentration gradient. It was found that a burst of drug was released in the first 3 h, an ideal drug release profile for several medical applications such as prevention of post-operation induced-adhesion because most infections occur within the first few hours after surgery. We speculate that as all charged ions are aggregated on the fiber surface, a great deal of drug molecules is on or near the fiber surface. We have tested this hypothesis by replotting the drug release data in the form of $\ln(M_t/M_\infty)$ versus time in Fig. 12C (M_t and M_∞ represent the drug concentrations in the solution at time t and at final time). If the release profile from the electrospun membrane is entirely due to the matrix diffusion, then a straight line is expected indicating Fickian diffusion. In Fig. 12C, it is clear that the relationship is non-linear, which indicates that drug release profile is not governed by the matrix diffusion alone. This is consistent with our hypothesis that a large amount of drug molecules is aggregated on or near the fiber surface by electrospinning.

Since the electrospun sample is porous, the overall drug

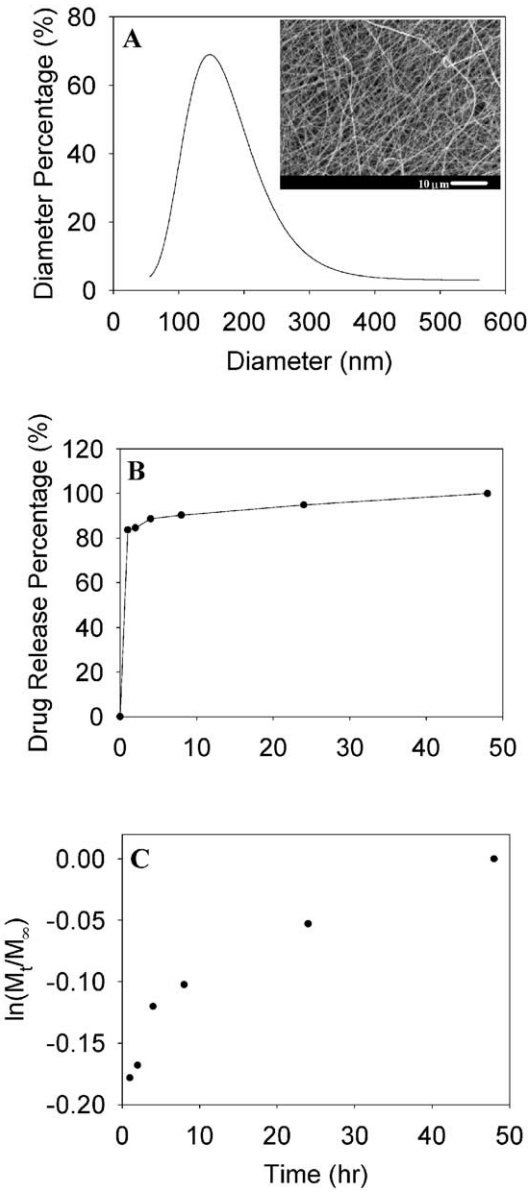

Fig. 12. (A) SEM images and diameter distribution of the membrane fabricated by electrospinning of a 30 wt% PDLA/DMF solution containing 1 wt% Mefoxin; (B) Mefoxin release profile from those membranes and (C) Mefoxin release profile in the logarithmic form to evaluate the nature of diffusion.

release flux from the membrane is much higher than that from the bulk films. From the release profile determined by UV spectroscopy, the drug loading efficiency of the electrospun PDLA membrane can be calculated by dividing the released amount by the initial loading amount. A typical loading efficiency of Mefoxin in the PDLA sample by electrospinning is over 90%. Finally, we wish to point out that the drug functionality seems to be completely unaffected by the gentle electrospinning process. In vitro and in vivo studies of the membranes containing Mefoxian have been carried out and will be published elsewhere.

4. Conclusions

The electrospinning technique was used to fabricate nanostructured bioabsorbable membranes for biomedical applications. The effects of solution properties and processing parameters on the structure and morphology of the electrospun membranes were thoroughly investigated. Results demonstrated that the morphology of electrospun polymer fibers depended on the strength of the electric field, the solution viscosity (e.g. concentration), the charge density of the solution (by salt addition), and the solution feeding rate. It was shown that higher concentration and higher charge density of the solution favored the formation of uniform nanofibers with no bead-like textures. The diameter of the nanofibers increased with electrospinning voltage as well as feeding rate of the solution. The effect of salt on the structure and morphology of the electrospun PDLA fibers is important since most drugs form charged ions in water. The addition of a small amount of salts or antibiotic drugs was found to greatly change the morphology of electrospun PDLA fibers from beads-on-fiber structure to uniform fiber-structure. The diameters of the nanofibers also decreased with the addition of salts. In addition, different salts exhibited different effects on the morphology of the electrospun fibers. The electrospinning of crystallizable PLLA resulted in a decrease of glass transition and crystallization temperatures, but an increase in the crystallization rate. Electrospinning was found to significantly retard the crystallization of PLLA. The amorphous phase in nascent electrospun PLLA membrane is probably not in a pure amorphous phase. Some metastable states, such as oriented chains with no helical structures, may exist in between the amorphous and crystalline states of electrospun PLLA fibers. In the present work, we focus on the effects of electrospinning processing on the structure and morphology of two types of PLA (non-crystallizable PDLA and crystallizable PLLA) non-woven membranes of nanofibers. In vitro studies dealing with degradation and mechanical properties of these electrospun PLA membranes, their relationships among structure, morphology, post treatments and properties have been carried out and will be discussed elsewhere.

Acknowledgments

The authors wish to thank Professor D. Reneker for providing valuable inspiration to this project and are grateful to Mr Greg Roduman for the help in taking SEM images. The authors also thank Dr Je-Young Kim and Ms Sharon Cruz for technical assistance. Financial support of this work was provided by the Center of Biotechnology at Stony Brook, a National Institute of Health-SBIR grant (GM63283-02) administered by the Stonybrook Technology and Applied Research Inc., the SUNY-SPIR program and the US Army Research Office (DAAD190010419).

References

[1] Chu CC. Biomed Engng Handbook 1995;P611.
[2] Langer R, Vacanti JP. Tissue Engng Sci 1993;260:920–6.
[3] Hermann JB, Kelly RJ, Higgins GA. Arch Surg 1970;486:100.
[4] King E, Cameron RE. J Appl Polym Sci 1997;66:1681–90.
[5] Zong XH, Wang ZG, Hsiao BS, Chu B, Zhou JJ, Jamiolkowki DD, Eugene M, Dormier E. Macromolecules 1999;32(24):8107–14.
[6] Butler SM, Tracy MA, Tilton RD. J Controlled Release 1999;58(3): 335–47.
[7] Esposito E, Cortesi R, Cervellati F, Menegatti E, Nastruzzi C. J Microencapsulation 1997;14(2):175–87.
[8] Zeleny J. Phys Rev 1914;3:69–91.
[9] Formhals A. Process and apparatus for preparing artificial threads. US Patent No. 1,975,504, 1934.
[10] Taylor GI. Proc R Soc Lond A 1964;280:383–97.
[11] Taylor GI. Proc R Soc Lond A 1969;31:453–75.
[12] Garton CG, Krasucki Z. Proc R Soc Lond A 1964;280:211–26.
[13] Doshi J, Reneker DH. J Electrostat 1995;35:151–60.
[14] Reneker DH, Yarin AL, Fong H, Koombhongs S. J Appl Phys 2000; 87(9):4531–47.
[15] Shin YM, Hohman MM, Brenner MP, Rutledge GC. Polymer 2001; 42(25):9955–67.
[16] Deitzel JM, Kleinmeyer JD, Hirvonen JK, Beck Tan NC. Polymer 2001;42(19):8163–70.
[17] Buchko CJ, Chen LC, Shen Y, Matin DC. Polymer 1999;40(26): 7397–407.
[18] Liu W, Wu Z, Reneker DH. Polym Prepr 2000;41(2):1193–4.
[19] Larrondo L, John Manley R. J Polym Sci, Polym Phys Ed 1981;19: 909–20.
[20] Ikada Y, Jamshidi K, Tsuji H, Hyon SH. Macromolecules 1987;20: 904–6.
[21] Ran SF, Zong XH, Fang DF, Hsiao BS, Chu B. Macromolecules 2001; 34(8):2569–78.
[22] Ran SF, Fang DF, Zong XH, Hsiao BS, Chu B. Polymer 2001;42(4): 1601–12.